

## RESEARCH ARTICLE

10.1002/2015JD024549

## Special Section:

East Asian Study of  
Tropospheric Aerosols and  
Impact on Cloud and  
Precipitation

## Key Points:

- Anthropogenic influences the DTR trend over Asia significantly
- Aerosol forcing is a major factor to the decreasing trend in the DTR over China
- Aerosol lowers  $T_{\max}$  in cities more than in rural areas

## Correspondence to:

Z. Li,  
zli@atmos.umd.edu

## Citation:

Liu, L., Z. Li, X. Yang, H. Gong, C. Li, and A. Xiong (2016), The long-term trend in the diurnal temperature range over Asia and its natural and anthropogenic causes, *J. Geophys. Res. Atmos.*, 121, 3519–3533, doi:10.1002/2015JD024549.

Received 23 NOV 2015

Accepted 16 MAR 2016

Accepted article online 24 MAR 2016

Published online 6 APR 2016

## The long-term trend in the diurnal temperature range over Asia and its natural and anthropogenic causes

Lin Liu<sup>1</sup>, Zhanqing Li<sup>1,2,3</sup>, Xin Yang<sup>1</sup>, Hainan Gong<sup>3</sup>, Chao Li<sup>4</sup>, and Anyuan Xiong<sup>5</sup>

<sup>1</sup>State Key Laboratory of Earth Surface Processes and Resource Ecology and College of Global Change and Earth System Science, Beijing Normal University, Beijing, China, <sup>2</sup>University of Maryland, College Park, Maryland, USA, <sup>3</sup>Center for Monsoon System Research, Institute of Atmospheric Physics, Chinese Academy of Sciences, Beijing, China, <sup>4</sup>Max Planck Institute for Meteorology, Hamburg, Germany, <sup>5</sup>National Meteorological Information Centre, Chinese Meteorological Administration, Beijing, China

**Abstract** Understanding the causes of long-term temperature trends is at the core of climate change studies. Any observed trend can result from natural variability or anthropogenic influences or both. In the present study, we evaluated the performance of 18 climate models from the Coupled Model Intercomparison Project Phase 5 on simulating the Asian diurnal temperature range (DTR) and explored the potential causes of the long-term trend in the DTR by examining the response of the DTR to natural forcing (volcanic aerosols and solar variability) and anthropogenic forcing (anthropogenic greenhouse gases (GHG) and aerosols) in the historical period of 1961–2005. For the climatology, the multimodel ensemble mean reproduced the geographical distribution and amplitude of the DTR over eastern China and India but underestimated the magnitudes of the DTR over the Tibetan Plateau and the high-latitude regions of the Asian continent. These negative biases in the DTR over frigid zones existed in most models. Seasonal biases in the DTR pattern from models were similar to the bias in the annual mean DTR pattern. Based on three selected state-of-the-art models, the observed decreasing trend in the DTR over Asia was reasonably reproduced in the all-forcing run. A comparison of separate forcing experiments revealed that anthropogenic forcing plays the dominant role in the declining trend in the DTR. Observations and model simulations showed that GHG forcing is mainly responsible for the negative trends in the DTR over Asia but that anthropogenic aerosol forcing was also behind the decreasing trend in the DTR over China and especially over eastern China.

### 1. Introduction

The observed increase in global average surface air temperatures since the midtwentieth century has been attributed to the increase in anthropogenic forcings [Meehl *et al.*, 2004; Intergovernmental Panel on Climate Change (IPCC), 2013]. The global mean warming trend over land has been associated with asymmetric changes in minimum and maximum surface temperatures. A greater warming has been observed in  $T_{\min}$  than in  $T_{\max}$ , inducing a decrease in the diurnal temperature range (DTR) on a global scale over the past several decades [Karl *et al.*, 1993; Dai *et al.*, 1999; Vose *et al.*, 2005]. The observed DTR trend may be affected by the large-scale effects of increasing aerosols and greenhouse gases (GHG) and also by regional changes in land surface processes [Collatz *et al.*, 2000; Zhou *et al.*, 2004, 2007, 2008]. General circulation models are generally able to capture the observed warming in recent decades when natural and anthropogenic forcings are included [IPCC, 2013]. Models have also revealed a decreasing trend in the DTR but with a much smaller magnitude than that found in observations [Stenchikov and Robock, 1995; Stone and Weaver, 2002, 2003; Karoly *et al.*, 2003; Braganza *et al.*, 2004; Zhou *et al.*, 2009a; Lewis and Karoly, 2013].

Given that many of the factors that influence the DTR have strong regional variations and that the anthropogenic effect is strongest in Asia, the ability of models in reproducing the climatology and long-term trends of the DTR is particularly challenging. One factor that could have a strong influence on the DTR is aerosols. Aerosols, whose concentration is particularly high over Asia, and especially over China and India [Li *et al.*, 2015], can influence global and regional climate significantly [e.g., Li *et al.*, 2011a, 2011b].

Due to the strong regional effect of aerosols, it is relatively easier to identify and isolate anthropogenic factors that induce biases in model performance, which is important for the improvement of models. Therefore, it is necessary to evaluate these basic aspects of the DTR in Coupled Model Intercomparison Project Phase 5

(CMIP5) models. In this study, we will try to address these questions: How well do the CMIP5 models reproduce the observed mean DTR state and its long-term trend over Asia, and how much do anthropogenic factors (GHG and aerosols) contribute to the trend? Some studies have suggested that the observed global trend in the DTR is caused by anthropogenic forcing to a great extent [e.g., Zhou *et al.*, 2010; Lewis and Karoly, 2013]. However, the relative contributions of GHG forcing and anthropogenic aerosol forcing on the DTR trend over Asia, where industrial growth at an unprecedented rate has taken place in the last few decades, remains unclear.

This study further examines the relative contributions of natural, GHG, and anthropogenic aerosols to the long-term trend in the DTR over Asia in recent decades based on outputs from the latest CMIP5 climate models. The rest of this paper is organized as follows. Section 2 describes the observed data sets, the CMIP5 models, and the analysis methods. Evaluations of the climatology of the DTR and the different contributions of natural, GHG, and aerosol forcings to changes in the DTR over Asia are presented in section 3. A summary and discussion are given in section 4.

## 2. Data, Model Experiments, and Method

### 2.1. Observations

Monthly mean observed daily near-surface minimum temperature ( $T_{\min}$ ) and near-surface maximum temperature ( $T_{\max}$ ) over land used in this study are from the Climatic Research Unit (CRU) high-resolution gridded data set, version 3.22 (CRU TS v.3.22), which has a horizontal resolution of  $0.5^\circ \times 0.5^\circ$  [Mitchell and Jones, 2005; Harris *et al.*, 2014]. Climatological DTR values are mainly from the Hadley Centre Global Climate Extremes Index 2 (HadEX2) product, which has a horizontal resolution of  $3.75^\circ \times 2.5^\circ$ . Donat *et al.* [2013] showed that the HadEX2 stations data are assessed more rigorously for both quality and homogeneity prior to gridding than other data sets.

To further single out the effect of anthropogenic aerosols on the DTR trend, homogenized daily climate data from observation stations provided by the National Meteorological Information Center of the China Meteorological Administration were also used. The inhomogeneity of data due to the relocations of station, the changes of observational instruments, and computation methods have been corrected [Wang *et al.*, 2007; Wang, 2008a, 2008b].

### 2.2. Model Experiments

CMIP5 models include different types of experiments: the historical experiment (Historical) including all forcings, the nature forcing experiment (HistNat) including solar radiation variability and volcanic aerosols, and the GHG forcing experiment (HistGHG) which is forced by well-mixed GHG changes. Eighteen historical simulations from 18 CMIP5 models were analyzed. The differences among realizations of the same model mainly denote the internal variability. The CMIP5 multimodel spread thus encompasses both the internal variability and response uncertainty. To make the analysis more concise, we choose only one realization from each model to evaluate the overall performances of the models in simulating the DTR over Asia. The HistGHG and HistNat experiments of models are also employed to analyze the relative contribution of nature and anthropogenic forcing on DTR trend over Asia. Detailed descriptions of the models are listed in Table 1.

### 2.3. Methods

In this study, the monthly mean DTR data are used which are the differences between the monthly means of  $T_{\max}$  and  $T_{\min}$  for both observations and models data. Following Taylor *et al.* [2012], the response to anthropogenic forcing is calculated as the difference between all forcing and natural forcing. The response of aerosol forcing is calculated as the difference between anthropogenic forcing and GHG forcing. For ease of comparison, all models and CRU data were bilinearly interpolated to a resolution of  $3.75^\circ \times 2.5^\circ$ . Analyses of observations and CMIP5 models results are from 1961 to 2005. Spring, summer, autumn, and winter means are constructed by averaging monthly mean data from March–May (MAM), June–August (JJA), September–November (SON), and December–February (DJF), respectively. A linear regression analysis was done and the significance of the results was assessed with a two-tailed Student's *t* test. The multimodel ensemble (MME) was calculated by averaging the variables over all the models with equal weighting. The intermodel uncertainty was assessed using the standard deviation of the models' performances.

**Table 1.** The CMIP5 Models Used in This Study<sup>a</sup>

Model	Research Center	Atmospheric Resolution
BCC-CSM1.1	Beijing Climate Center, China Meteorological Administration	128 × 64 L26
CanESM2	Canadian Centre for Climate Modelling and Analysis	128 × 64 L35
CCSM4	National Center for Atmospheric Research	288 × 192 L26
CESM1-CAM5	Community Earth System Model Contributors	288 × 192 L30
CNRM-CM5	Centre National de Recherches Météorologiques/Centre Européen de Recherche et Formation Avancée en Calcul Scientifique	256 × 128 L31
CSIRO-Mk3.6.0	Commonwealth Scientific and Industrial Research Organization in collaboration with Queensland Climate Change Centre of Excellence	192 × 96 L18
EC-EARTH	EC-EARTH consortium	320 × 160 L62
FGOALS-g2	LASG, Institute of Atmospheric Physics, Chinese Academy of Sciences and CESS, Tsinghua University	128 × 60 L26
GISS-E2-H	NASA Goddard Institute for Space Studies	144 × 90 L40
GISS-E2-R	NASA Goddard Institute for Space Studies	144 × 90 L40
HadCM3	Met Office Hadley Centre (additional HadGEM2-ES realizations contributed by Instituto Nacional de Pesquisas Espaciais)	96 × 73 L19
HadGEM2-CC	Met Office Hadley Centre (additional HadGEM2-ES realizations contributed by Instituto Nacional de Pesquisas Espaciais)	192 × 144 L60
MIROC5	Atmosphere and Ocean Research Institute (The University of Tokyo), National Institute for Environmental Studies, and Japan Agency for Marine-Earth Science and Technology	256 × 128 L40
MIROC-ESM	Japan Agency for Marine-Earth Science and Technology, Atmosphere and Ocean Research Institute (The University of Tokyo), and National Institute for Environmental Studies	128 × 64 L80
MPI-ESM-LR	Max-Planck-Institut für Meteorologie (Max Planck Institute for Meteorology)	192 × 96 L47
MPI-ESM-MR	Max-Planck-Institut für Meteorologie (Max Planck Institute for Meteorology)	192 × 96 L95
MRI-CGCM3	Meteorological Research Institute	320 × 160 L48
NorESM1-M	Norwegian Climate Centre	144 × 96 L26

<sup>a</sup>The horizontal resolution (longitude × latitude grids) and vertical levels (L) of each model are also listed.

### 3. Results

#### 3.1. The Climatology of the DTR From CMIP5 Models

Figures 1a and 1b show the geographical distributions of annual mean DTR from the HadEX2 data set (hereafter referred to as “observations”) and the MME of 18 CMIP5 models, respectively. From observations (Figure 1a), larger DTRs are seen from Lake Baikal to India. DTRs greater than 12°C and with maxima in the 16–18°C range are also seen in northwest China and the Middle East. Low values are mainly found over the high-latitude regions of the Eurasian continent and eastern China. The geographical differences in the DTR may be related to the spatial distribution of aerosol concentration, cloud cover, precipitation, surface soil moisture, and vegetation cover, etc. [e.g., Sun *et al.*, 2006; Zhou *et al.*, 2009b, 2010]. The MME (Figure 1b) clearly captures the main features over eastern China, the Middle East, and India. However, the DTRs over the Tibetan Plateau and north of 40°N in Asia are substantially underestimated by 2–4°C compared with observations (Figure 1c). Figure 1d shows the intermodel uncertainty as represented by the intermodel variance. The intermodel spreads of the DTR are small over eastern China but are larger over western China, northern India, and the Middle East, which are arid or semiarid regions. Surface processes such as soil moisture play an important role in the DTR in arid and semiarid regions [e.g., Wang *et al.*, 2014]. Different treatments of land processes in the models might be one of the reasons for the differences seen in simulations of the DTR over dry regions by the different models.

Because the distribution of the DTR has seasonal patterns, the climatology of seasonal mean DTR over Asia was evaluated (Figure 2). The observed DTR patterns in different seasons are similar, but some differences are seen. The seasonal change in the DTR over India is clearly seen from observations. In JJA, the DTR is smallest (Figure 2e) and steadily increases from JJA to MAM (Figures 2a, 2e, 2i, and 2m). This change in the DTR is related to changes not only in cloud cover and soil moisture due to the wet and dry transitions but also to aerosols which have the strongest effect on maximum temperatures in summer [Dai *et al.*, 1997, 1999; Leibensperger *et al.*, 2012; Yang *et al.*, 2013]. The MME captures the seasonal change in the DTR over India and the intensities of the DTR, in general, when compared to observations. The DTR from the MME is slightly larger over northern India in MAM and JJA than the observations (Figures 2c and 2g). As with the annual mean, the MME also underestimates the DTR north of 40°N over continental Asia and western

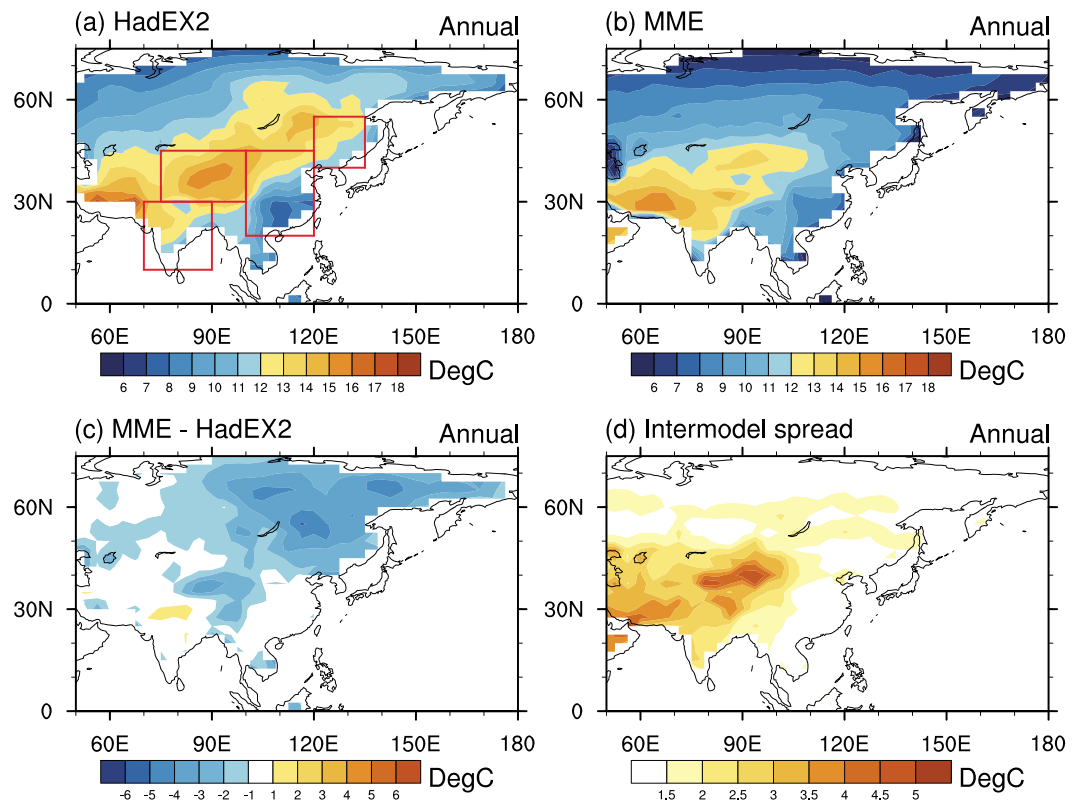


**Figure 1.** (a) Climatology (1961–2005) of annual mean DTR based in the HadEX2 data set, (b) as in Figure 1a but for the MME of 18 CMIP5 models, (c) the difference between Figures 1b and 1a, and (d) intermodel standard deviation of the DTR from 18 CMIP5 models. The red boxes in Figure 1a outline the four subregions used in a later analysis.

China (Figures 2c, 2g, 2k, and 2o) and has a larger intermodel uncertainty over western China and northern India in all seasons (Figure 2d, 2h, 2l, and 2p). These results suggest that there are some common model biases and intermodel uncertainties in annual mean and seasonal DTR simulations.

Taylor diagrams can succinctly describe the coherence between models and observations in terms of the root-mean-square difference, the spatial pattern correlation, and the ratio of their standard deviations [Taylor, 2001]. To assess the performances of the 18 CMIP5 models in representing the DTR climatology over Asia in more detail, Taylor diagrams (Figure 3) are plotted for Asia (10°–55°N, 70°–135°E), which contains the major regions of mainland China and India. The correlation coefficients from least squares fittings to the relationships between modeled climatological DTRs and observations range from 0.4 to 0.8. The spatial standard deviations of the model data are slightly lower than that of observations. The pattern correlation between the MME and observations is 0.8, and its spatial standard deviation is also closer to observations. The CanESM2, CNRM-CM5, and HadCM3 models have much larger spatial standard deviations than do observations although their pattern correlations are comparable to the other models. This suggests that climatological DTR simulations are reasonable because the pattern correlation coefficients are comparable with those in large-scale circulations [Gong et al., 2014].

The Taylor diagram can show the resemblance between different spatial patterns but it cannot describe the differences in absolute intensity of the DTR, so we further examine the intensity of the DTR by calculating the differences between model outputs and observations. Mainland China and India are first divided into four subregions: middle eastern China (MEC), northeastern China (NEC), western China (WC), and India (IND). The four regions are outlined in red in Figure 1a. Figure 4 shows the differences in the annual mean DTR between observations and the 18 CMIP5 models in the four regions. The observed annual mean DTR is 10.8°C, 12.4°C, 13.9°C, and 12.1°C in the MEC, NEC, WC, and IND regions, respectively. The DTR is highest in the WC region where the climate is arid or semiarid and lowest in the relatively humid MEC region. This agrees with earlier studies that have shown that the maximum temperature is reduced through cloud radiative and evaporative cooling effects,

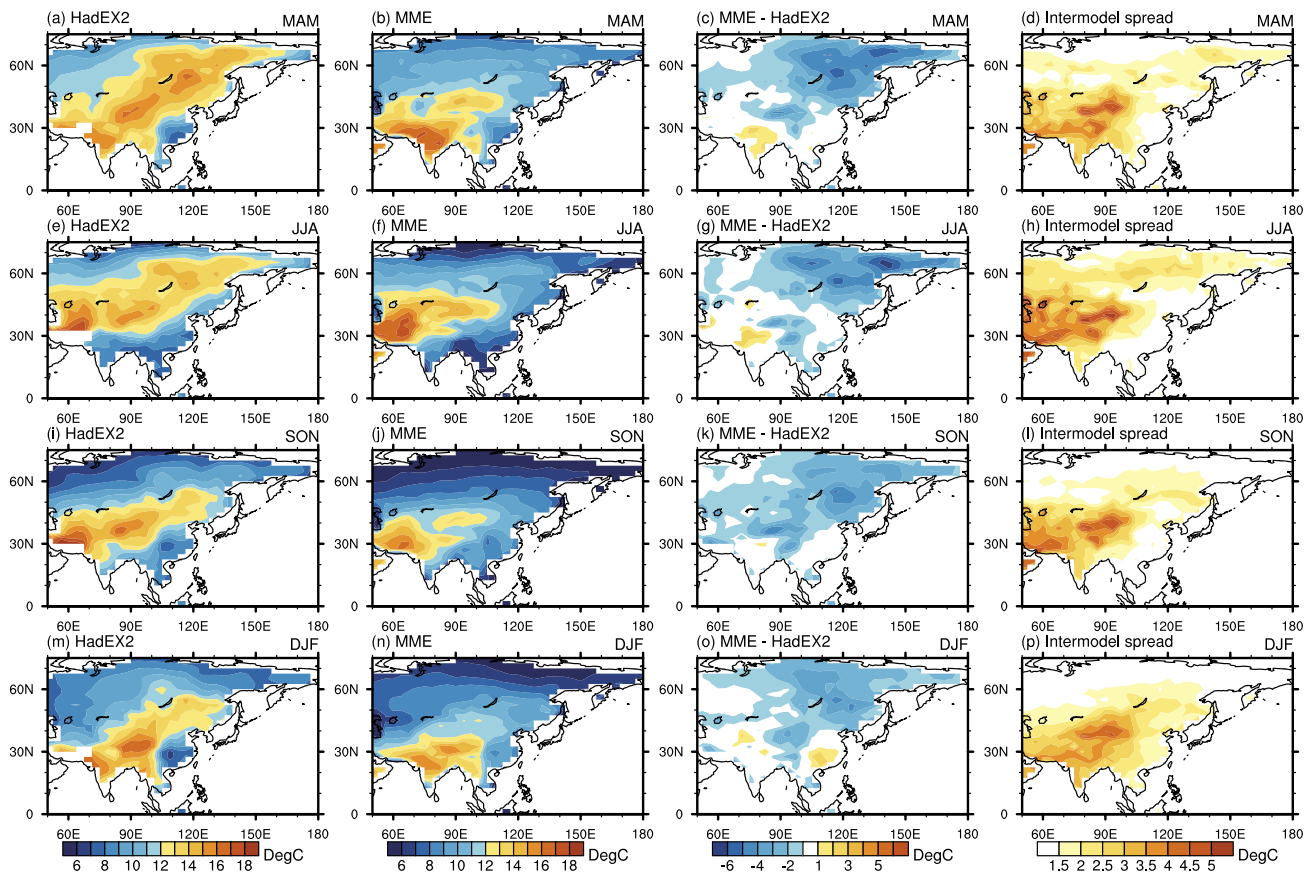


**Figure 2.** As in Figure 1 but for (a–d) MAM, (e–h) JJA, (i–l) SON, and (m–p) DJF.

which results in a smaller DTR in humid regions (Figure 4). DTR biases over the MEC, NEC, WC, and IND regions in the MME are  $-0.9^{\circ}\text{C}$ ,  $-3.1^{\circ}\text{C}$ ,  $-1.1^{\circ}\text{C}$ , and  $-0.2^{\circ}\text{C}$ , respectively. The relatively small DTR bias over India suggests that the MME of CMIP5 models can reproduce well the DTR over India (Figure 4d). Negative biases are seen over the other three regions (Figures 4a–4c). In the MEC region, 17 of the 18 models show negative biases (Figure 4a). Only the CNRM-CM5 model shows a positive bias ( $\sim 2^{\circ}\text{C}$ ). In the WC region, only three models (CanESM2, CNRM-CM5, and HadCM3) show positive biases (Figure 4c). The strongest negative biases are seen in the NEC region (Figure 4b). These results suggest that the climatological strengths of the DTR over the MEC, NEC, and WC regions are underestimated by most of the models. The causes for these biases are not clear, but they might be associated with cloud cover, precipitation, the treatment of land processes in models, and anthropogenic aerosol effects [Lindvall and Svensson, 2015].

The DTR in different seasons from observations has different intensities due to the different climate conditions (Figure 5). The climatological DTR is smallest over all four regions, especially over India, in JJA due to the relatively wet conditions present then (Figures 5e–5h). Summer is the rainy season in India. Increased rain in the daytime and increased clouds at night can both contribute to the declining trend in summer DTR over India (Figure 5h). Modeled climatological DTR seasonal biases behave in a similar manner as annual mean climatological DTR biases. The MME reproduces well the DTR over the WC and IND regions in summer (Figures 5g and 5h) and the MEC region in winter.

### 3.2. The Long-Term Trend in the DTR and Its Characteristics

The long-term trend in the DTR from both observations and model outputs is analyzed so that the natural and anthropogenic signals in simulated DTR trends over mainland China and India from 1961 to 2005 can be detected. Major features of the trend in the DTR on an annual basis and seasonally are similar. So the focus is placed on analyzing the trend in the annual mean DTR only. Table 2 lists the trends in the annual mean DTR from the HadEX2 and CMIP5 models in each region based on data from 1961 to 2005. The observed DTR

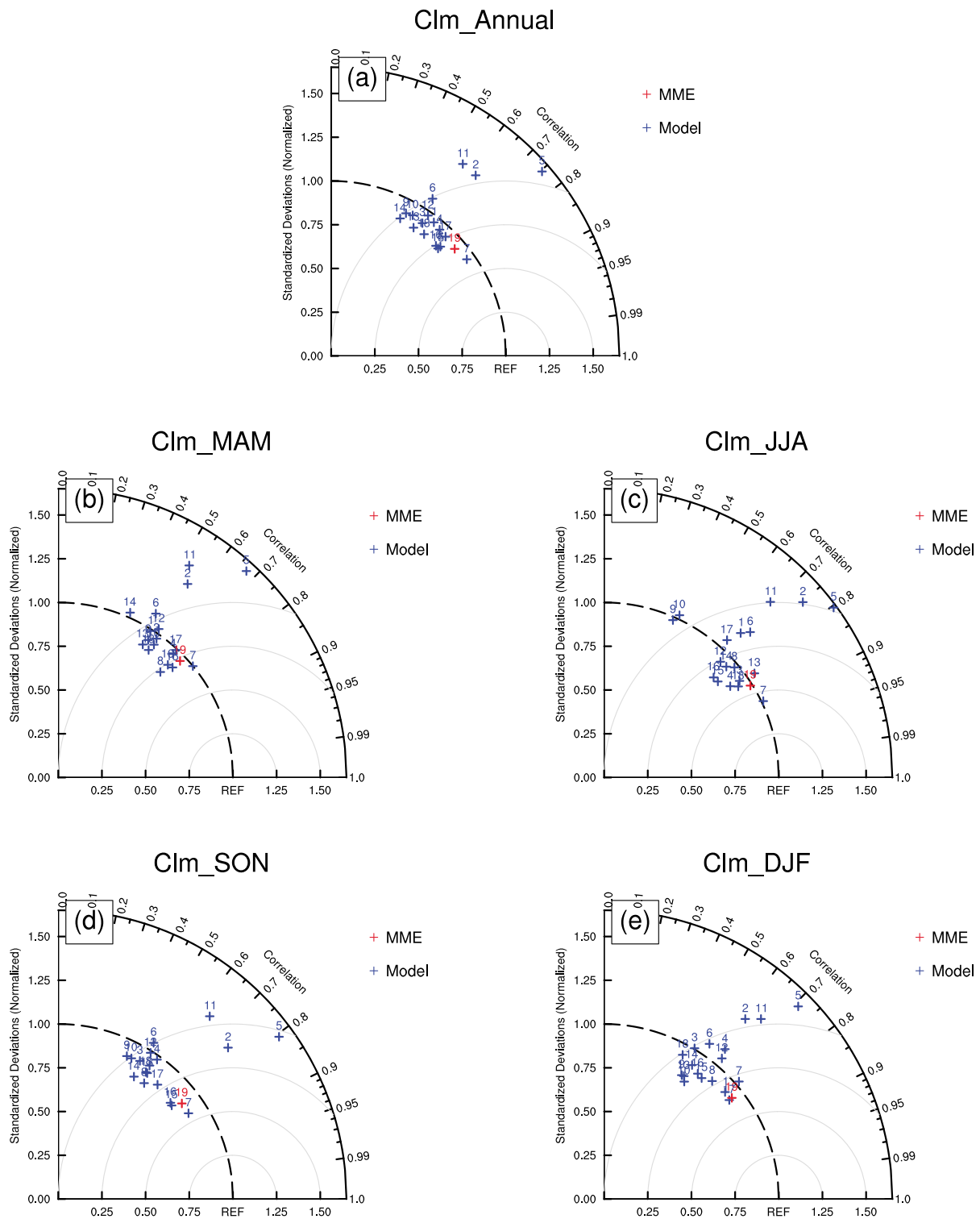


**Figure 3.** Taylor diagrams of annual and seasonal climatologies of the DTR over Asia ( $10^{\circ}$ – $55^{\circ}$ N,  $70^{\circ}$ – $135^{\circ}$ E) based on 45 years (1961–2005) of data. Red crosses represent results from the MME, and blue crosses represent results from each model.

shows a significant negative trend over Asia, which has a magnitude of  $-0.70^{\circ}\text{C}$ ,  $-0.79^{\circ}\text{C}$ ,  $-0.79^{\circ}\text{C}$ , and  $-0.34^{\circ}\text{C}$  over the 45 year period for the MEC, NEC, WC, and IND regions, respectively (all exceeding the 95% confidence level). Most of the models can simulate the negative trend in the DTR in each region over the time period chosen, but the magnitudes of the trends are smaller than those from observations. This

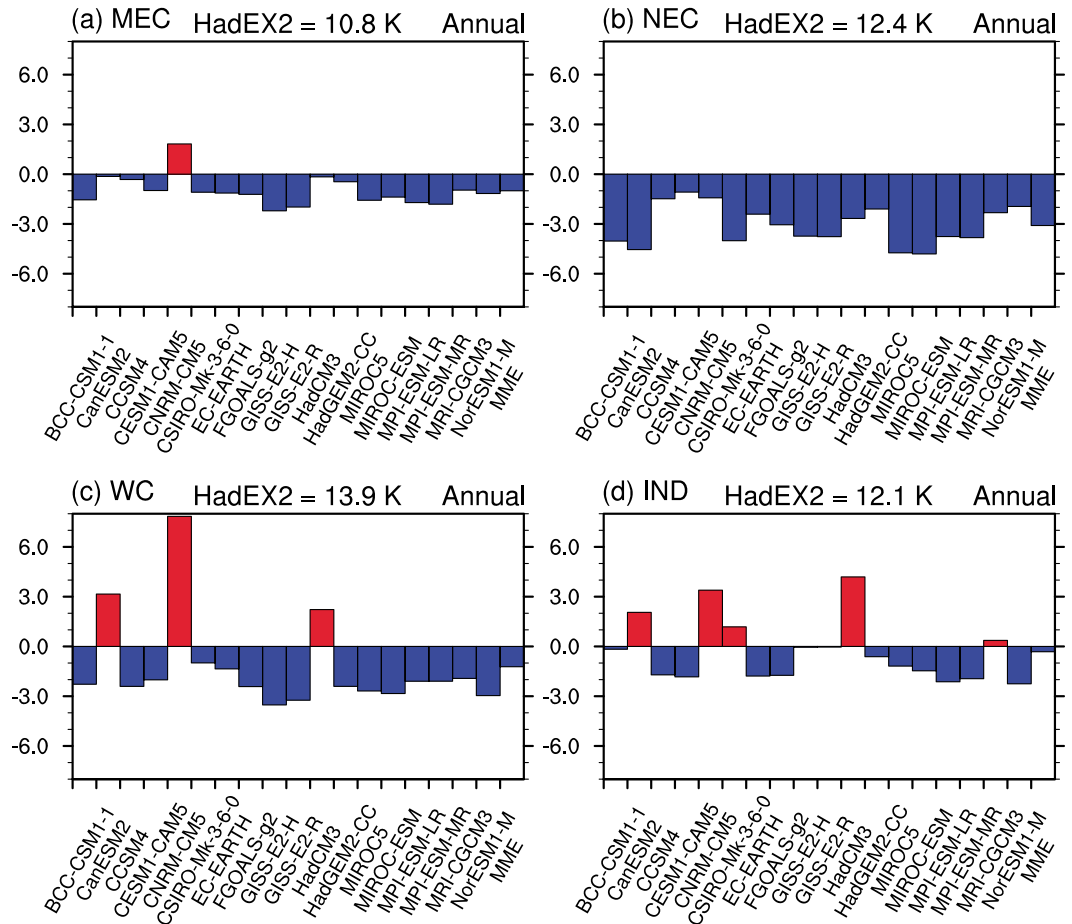


**Figure 4.** Differences (K) in climatological annual mean DTR between 18 CMIP5 models and HadEX2 data for the (a) MEC, (b) NEC, (c) WC, and (d) IND regions.

result confirms the findings of *Lewis and Karoly* [2013]. The one exception is the GISS-E2-R model, which shows a positive DTR trend in all four regions. The CNRM-CM5, MIROC-ESM, and MRI-CGCM3 model-simulated trends are closest to the observed trend. Therefore, these three models are next chosen to analyze the relative contributions of different forcings to the DTR trend.

Much research has shown that anthropogenic forcing factors such as GHG and aerosols can also affect the trend in the DTR. A rapid increase in aerosol loading can mask the warming effect of GHG to some extent. Here the different forcing runs from the MME of the three models are analyzed to investigate their contributions to the declining trend in the DTR over Asia. Due to the unavailability of monthly mean  $T_{max}$  and  $T_{min}$  in the HadEX2 data set, the CRU TS v.3.22 data set is used to analyze the trends in the DTR,  $T_{max}$ , and  $T_{min}$ . Hereafter, the CRU data set represents observations. Figure 6 shows the spatial distribution of the linear trends in the DTR during 1961–2005 from observations and from different runs of the MME over Asia. Negative trends in the DTR are found over most of the Asian continent in both observations and the all-forcing run. The magnitudes of simulated negative DTR trends in the all-forcing run are smaller than that of observations (Figures 6a and 6b). This suggests that the weak negative trend in the DTR is a common bias of CMIP5 models. The DTR trend from the natural-forcing run is much weaker than the DTR trend from the all-forcing run (Figure 6c). In this case, the anthropogenic forcing run has a similar pattern in the annual mean DTR trend as the all-forcing run (Figures 6b and 6d). This result shows that anthropogenic forcing plays a dominant role in the declining trend in the DTR over Asia. In terms of the GHG forcing, the negative trend in the DTR covers most of the Asian continent and is significant over midwestern China, central Asia, northern India, southeastern Asia, and at high latitudes (Figure 6e). Compared with the GHG forcing run, the declining trends in the DTR are more significant over China, especially over eastern and northeastern China, in the

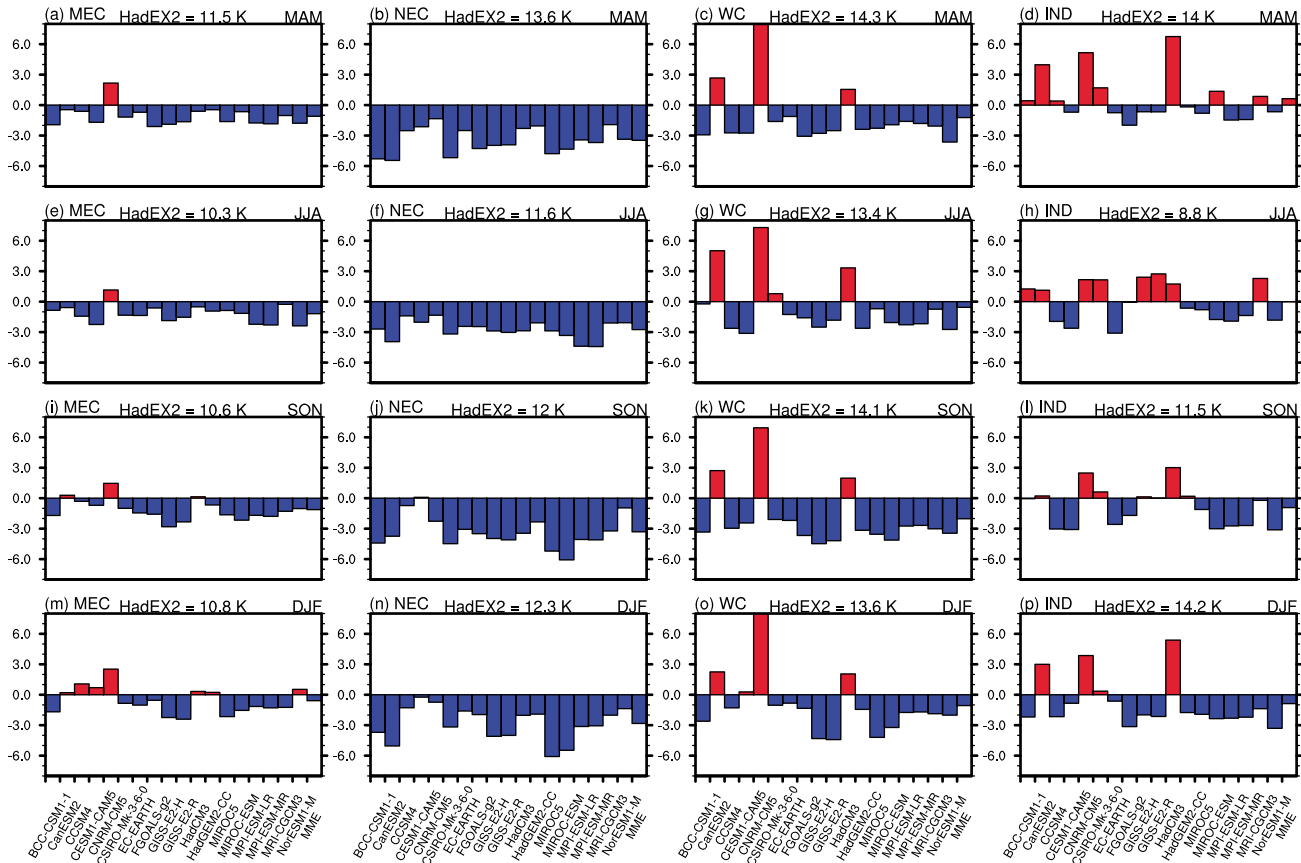


Figure 5. As in Figure 4 but for (a–d) MAM, (e–h) JJA, (i–l) SON, and (m–p) DJF.

Table 2. Trends (K per 45 Years) in Annual Mean DTR From Observations and 18 CMIP5 Models<sup>a</sup>

Obs/Model	MEC	NEC	WC	IND
HadEx2	-0.70**	-0.79**	-0.79**	-0.34*
BCC-CSM1-1	-0.05	-0.19	-0.06	-0.13
CanESM2	-0.28	-0.05	-0.52**	-0.16
CCSM4	-0.20	-0.20	-0.14	-0.21
CESM1-CAM5	-0.37*	-0.17	-0.37**	-0.12
CNRM-CM5	-0.44**	-0.44**	-0.58**	-0.14
CSIRO-MK-3-6-0	0.03	0.02	-0.48**	-0.29*
EC-EARTH	-0.27*	-0.18	-0.26*	-0.02
FGOALS-g2	-0.17	0.05	-0.36**	-0.14
GISS-E2-H	-0.33**	-0.34**	0.19**	0.03
GISS-E2-R	0.21*	0.07	0.14	0.15
HadCM3	-0.23	-0.53**	-0.45*	-0.36
HadGEM2-CC	-0.01	-0.09	-0.80**	-0.47*
MIROC5	-0.24*	-0.22	-0.10	-0.54**
MIROC-ESM	-0.24*	-0.41**	-0.18**	-0.12
MPI-ESM-LR	-0.03	-0.01	-0.05	-0.20
MPI-ESM-MR	-0.04	-0.11	-0.14	-0.22
MRI-CGCM3	-0.42**	-0.23*	-0.24**	-0.72**
NorESM1-M	-0.22*	-0.15	-0.04	-0.18

<sup>a</sup>MEC: Middle Eastern China, NEC: Northeastern China, WC: Western China, IND: India.

\*95% confidence levels.

\*\*99% confidence levels.

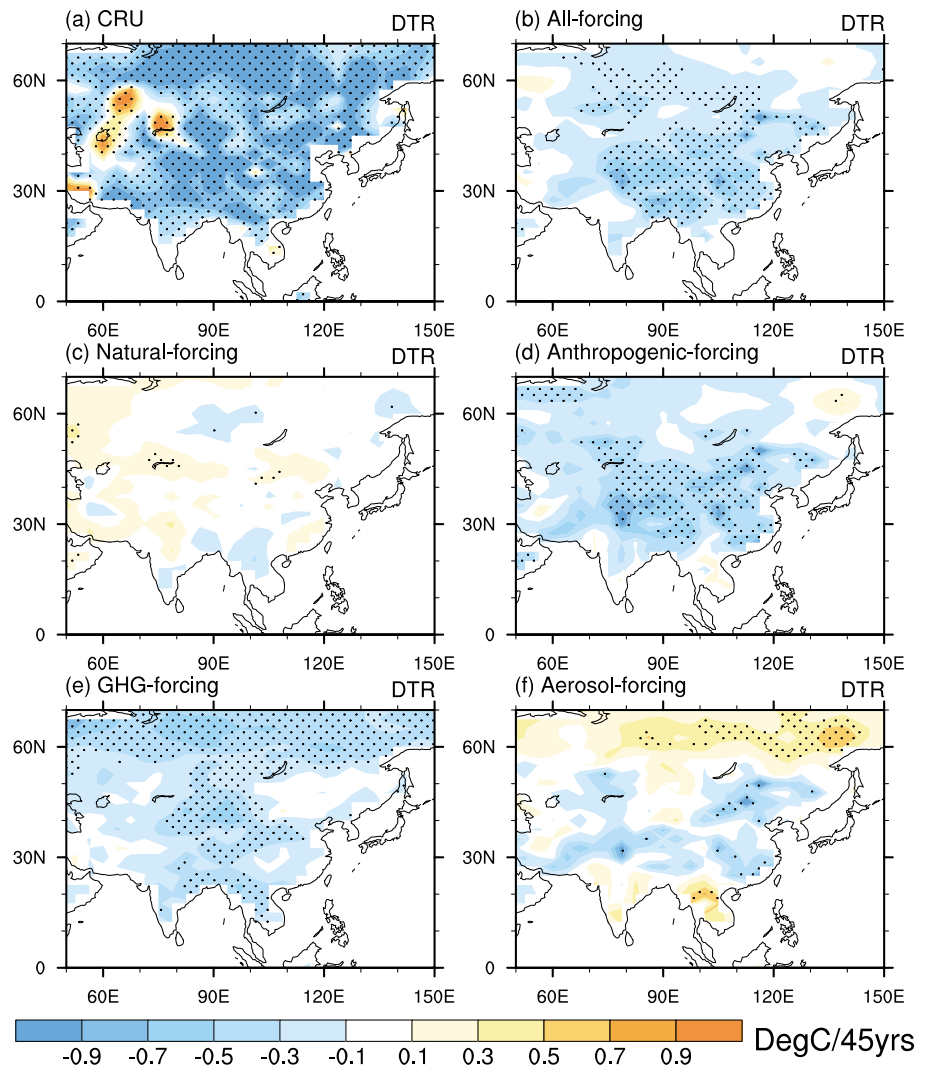


**Figure 6.** Linear trends in annual mean DTR (1961–2005) from (a) the CRU data set, (b) the all-forcing experiment, (c) the natural-forcing experiment, (d) the anthropogenic forcing experiment, (e) the GHG forcing experiment, and (f) the aerosol forcing experiment. Dotted areas show where trends in the DTR are statistically significant at the 90% level. The MME is constructed using the three CMIP5 models with the most similar simulated trends as the observed trend in the DTR.

anthropogenic aerosol forcing run (Figure 6f). This suggests that anthropogenic aerosol forcing plays a more important role in the decreasing trend in the DTR over China. GHG forcing is a major factor inducing the negative trend in the DTR over India. Significant positive trends in the DTR over southeastern Asia and at high latitudes are seen in the anthropogenic aerosol forcing run, which is contrary to the trends seen in the GHG forcing run (Figures 6e and 6f).

To determine the causes behind the strong declining trends in the DTR over Asia, linear trends in  $T_{max}$  and  $T_{min}$  in different forcing runs are shown in Figures 7 and 9, respectively. Figure 7 shows the spatial distributions of observed and simulated  $T_{max}$  trends over the period of 1961–2005. Positive trends in  $T_{max}$  from both observations and the all-forcing run are seen over most regions in Asia. The simulated trends in  $T_{max}$  in the all-forcing run generally capture observed large-scale features and some small-scale features, in particular, the weak trend in  $T_{max}$  over mideastern China (Figures 7a and 7b). The trend in  $T_{max}$  in the natural-forcing run (Figure 7c) is overall weaker than in the anthropogenic forcing run (Figure 7d). The anthropogenic forcing and all-forcing runs have similar patterns in the distribution of  $T_{max}$  (Figures 7b and 7d). This suggests that anthropogenic forcing plays a major role in the trend in  $T_{max}$  over Asia. A warming trend in  $T_{max}$  over Asia is seen in the GHG forcing run (Figure 7e) with increases toward higher latitudes.

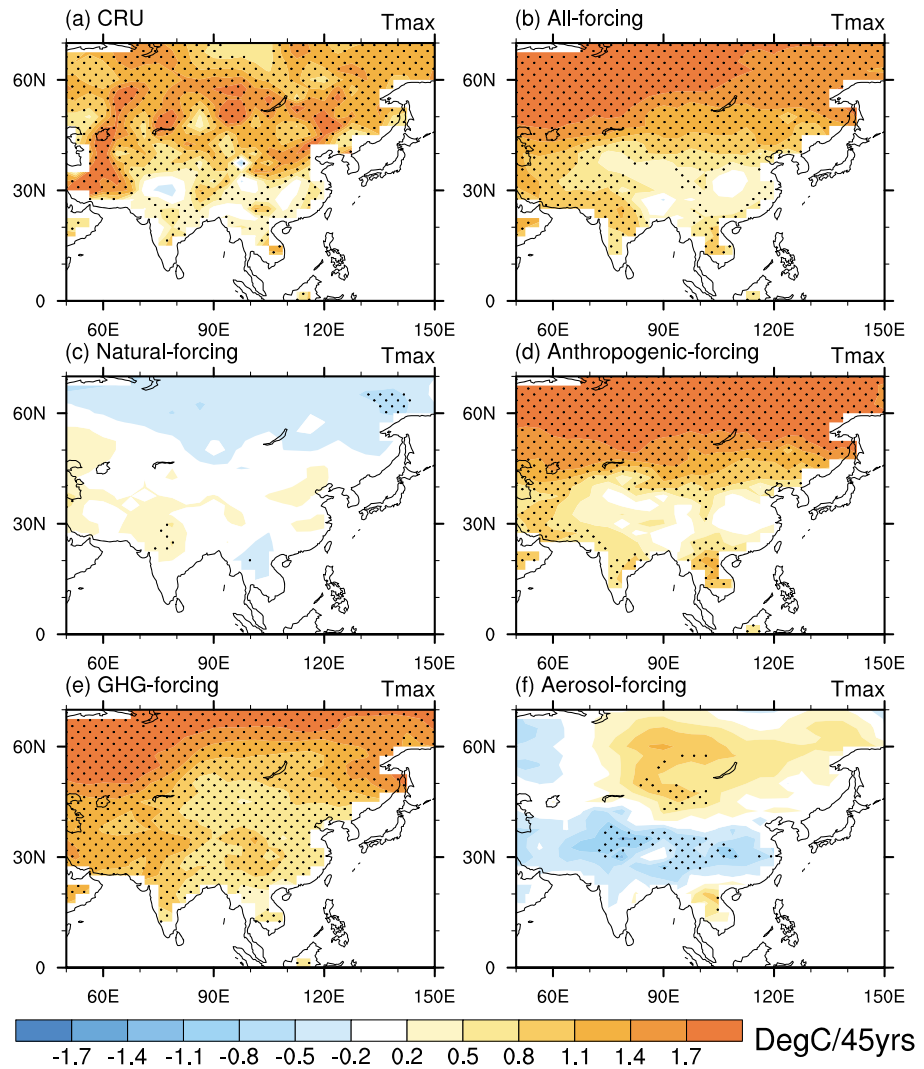
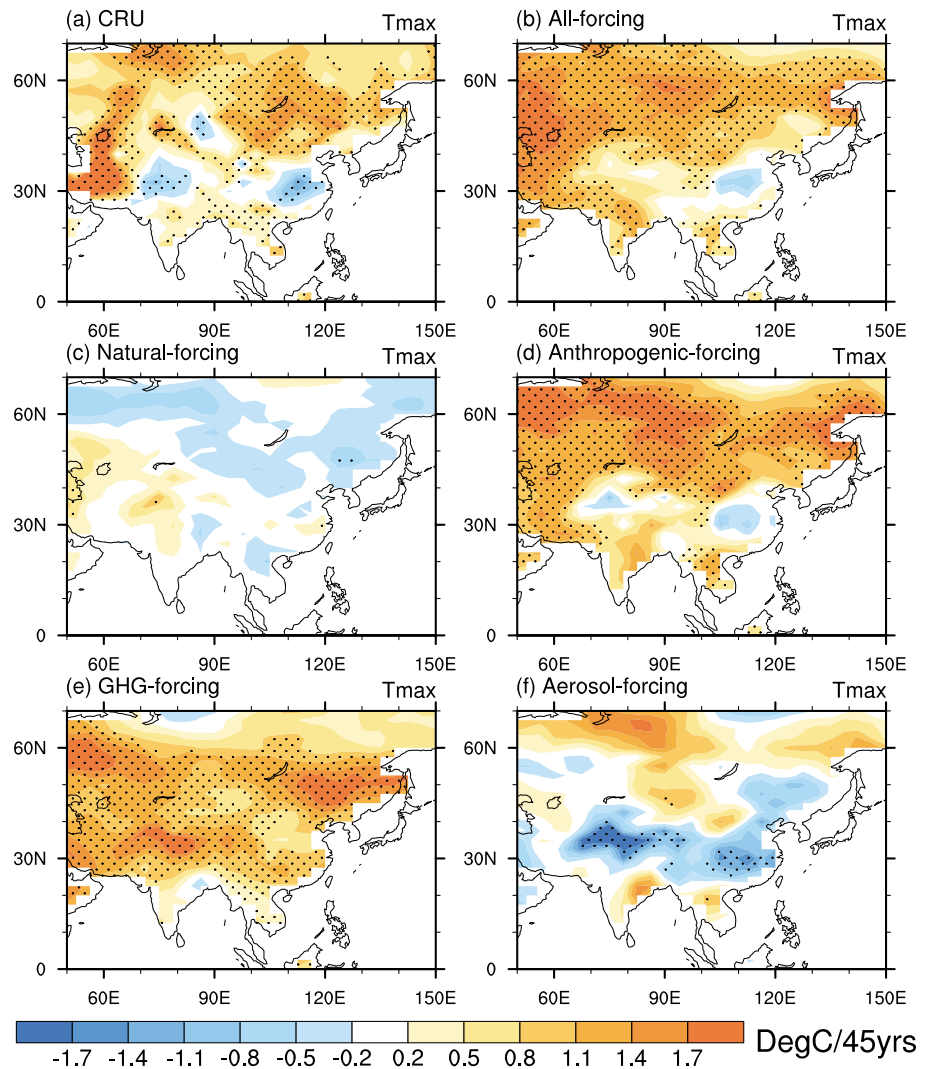


Figure 7. As Figure 6 but for  $T_{max}$ .

Over the southern part of the Asian continent, a cooling trend in  $T_{max}$  is seen in the anthropogenic aerosol forcing run (Figure 7f) as well as a warming trend in  $T_{max}$  over the inner regions of the Asian continent. The cooling effect of anthropogenic aerosol forcing on  $T_{max}$  counteracts the warming trend of GHG forcing to a great extent, which amounts to a negligible trend in  $T_{max}$  over eastern China from models. In JJA, negative trends in  $T_{max}$  are seen over eastern China both in observations and in the all-forcing run (Figure 8). The significant negative trend in  $T_{max}$  is mainly due to anthropogenic aerosol forcing in models. While anthropogenic aerosols may be heavier during winter over China, aerosol radiative forcing in winter is weaker than that in summer due to reduced solar insolation in winter and so is the winter trend. Based on the model results, we do see a relatively weak trend in annual mean  $T_{max}$  over eastern China as a result of this offsetting effect.

The spatial distributions of observed and simulated  $T_{min}$  trends are shown in Figure 9. Strong warming trends in  $T_{min}$  over the Asian continent can be seen in both observations and the all-forcing run. Simulated positive trends in  $T_{min}$  in the all-forcing run are smaller in magnitude than observed positive trends in  $T_{min}$ , especially over China (Figures 9a and 9b), which results in a weaker trend in the DTR from models than from observations over this region. Underestimation of the urbanization effect over China might be a reason for this bias [Zhou *et al.*, 2004; Ren *et al.*, 2008; Ren and Zhou, 2014]. As was seen for  $T_{max}$ , the trend in  $T_{min}$  in the natural-forcing run is much weaker compared with that in the anthropogenic forcing run, which also suggests that the trend in  $T_{min}$  is significantly affected by human activity and not by natural variability (Figures 9c and 9d). Although the spatial



**Figure 8.** As in Figure 7 but for JJA.

pattern of the  $T_{\min}$  trend is similar to that of the  $T_{\max}$  trend in the GHG forcing run, the magnitude of the  $T_{\min}$  trend is larger over most regions of the Asian continent (Figures 7e and 9e). There tends to be more downwelling longwave radiation at night than during the day [Lindvall and Svensson, 2015], especially at high latitudes and in midwestern China, which results in a negative trend in the DTR in the GHG forcing run. The spatial patterns of the  $T_{\min}$  and  $T_{\max}$  trends in the anthropogenic aerosol forcing run are similar, but some differences are seen (Figures 7f and 9f). The negative trend in  $T_{\min}$  is weaker and less significant than that in  $T_{\max}$  over eastern China, and the positive trend in  $T_{\min}$  over northeastern China is stronger and more significant than that in  $T_{\max}$ , which results in a significant declining trend in the DTR over eastern and northern China (Figures 7f and 9f).

### 3.3. Impact of the Aerosol Direct Effect on the DTR Trend Over China From Observations

Aerosols can influence surface temperature directly by scattering and absorbing solar radiation. This effect is strongest during the daytime and especially on  $T_{\max}$ . Historical records of temperature and visibility collected in China are used to validate our argument, or hypothesis, concerning the role of aerosols in the long-term trends in  $T_{\max}$  and the DTR. Any long-term trend in temperature may result from a combination of changes in many factors, such as natural variability on multiple time scales, the greenhouse effect, urbanization, and aerosols. It is generally very difficult to sort out the contributions of these factors to any observed trend. The method is simple but effective to single out the effect of aerosols by using temperature data at pairs of stations in close proximity but at different altitudes, i.e., stations located on mountain tops paired with

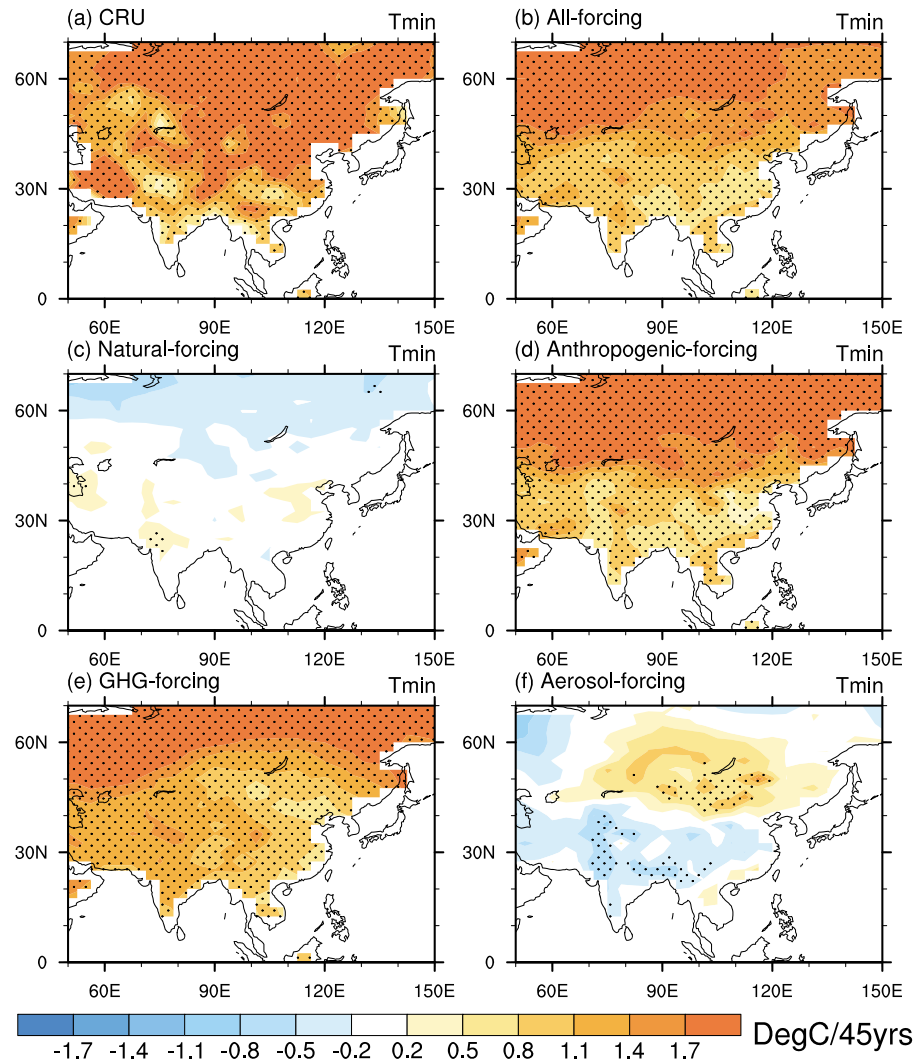


**Figure 9.** As Figure 6 but for  $T_{min}$ .

stations in the neighboring plains or valleys. The pairs of stations share a similar meteorology but have distinct aerosol loading which is much less at the top of high mountains than in the foothills [Yang *et al.*, 2013].

Differences in the trends in  $T_{max}$  and DTR between the low-land cities and nearby mountains were examined to identify the possible influence of aerosols, and the long-term trend of visibility is used as a proxy for aerosol loading which is only available over a long period. Two city/mountain pairs from rapidly developing industrial regions of China were first identified: Taiyuan/Mount Wutai in Shanxi Province and Xi'an/Mount Hua in Shaanxi Province. Mean visibilities on clear days based on observations made from 1980 to 2012 in Taiyuan/Mount Wutai and Xi'an/Mount Hua are 12.3/32.9 km and 13.9/22.5 km, respectively. The mountain stations are thus ideal for representing background conditions. Although the Mount Wutai station has been relocated from 2895.8 m to 2208.3 m in 1998, the influence of the relocation has been corrected during the processes of data homogenization. Figure 10a shows the time series of  $T_{max}$  from the Taiyuan and Mount Wutai stations on clear days from 1980 to 2012. The positive trend in  $T_{max}$  from Taiyuan is significantly smaller than that from Mount Wutai (Figure 10a). In the time series of maximum temperature at Mount Wutai station, there was no abrupt change near 1998, suggesting that the influence of station relocation on the data quality has been eliminated at the Mount Wutai station. Similar patterns are seen in the time series for Xi'an and Mount Hua (Figure 10b). Figure 10c shows the linear trends in  $T_{max}$  from the city and mountain stations and their differences. The trends in  $T_{max}$  from Taiyuan and Xi'an are 0.16°C per decade and 0.3°C per decade smaller than those from Mount Wutai and Mount Hua, respectively. This was accompanied by significant negative trends in visibility observed

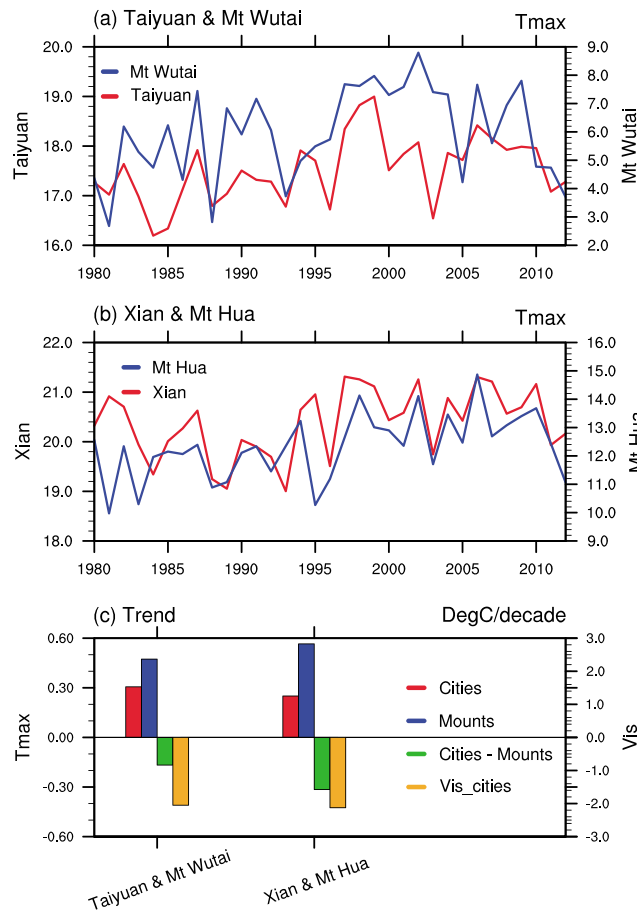


**Figure 10.** Time series of  $T_{max}$  (°C) from (a) Taiyuan (red line) and Mount Wutai (blue line) stations and (b) Xi'an (red line) and Mount Hua (blue line) stations on clear-sky days from 1980 to 2012. (c) Linear trends in  $T_{max}$  (°C per decade) from city and mountain stations (left ordinate, red and blue bars, respectively) and trends in visibility (km per decade) in the cities (right ordinate, yellow bars). Green bars show the difference between red and blue bars.

the models have low skill in simulating the DTR over arid and frigid zones. The treatment of land processes in these regions may be a possible reason for the common bias seen in model outputs.

Taylor diagrams show that the MME captured reasonably well both the spatial pattern and the spatial standard deviation in the annual DTR over mainland China and India. Three models (CanESM2, CNRM-CM5, and HadCM3) showed large spatial standard deviations in the annual DTR. Four regions located in mainland China and India were defined (MEC, NEC, WC, and IND). The MME reproduced the intensity of the annual DTR over IND relatively well, although negative biases were found in all four regions. The CNRM-CM5 model showed the strongest positive biases in the MEC, WC, and IND regions. All models showed a negative bias in the NEC region, which is partially located in a frigid zone. Seasonal biases were almost the same as the annual mean bias. This suggests that the models fail to capture the intensity of the annual DTR over the NEC.

Trends in the DTR over Asia using observations and CMIP5 model outputs for the period of 1961–2005 were also analyzed. Although most of the models simulated a negative trend in the DTR over Asia, the magnitude was underestimated. Based on three selected state-of-the-art models, the observed decreasing trend in the DTR over Asia was reasonably reproduced in the all-forcing run. A comparison of separate forcing experiments reveals that anthropogenic forcing plays the dominant role in the declining trend in the DTR. The negative trends in the DTR over Asia were mainly determined by GHG forcing, but anthropogenic aerosol forcing was mainly responsible for the decreasing trend in the DTR over China and especially over eastern China. The relatively weak trend in  $T_{max}$  over eastern China seen in both observations and the all-forcing

at Taiyuan (~2 km per decade) and at Xi'an (2.2 km per decade). These results suggest that the significant decreases in visibility presumably due to increases in aerosol concentration weakened the upward trends in  $T_{max}$  by the greenhouse effect in cities and thereby contributed to the reduction in the DTR. This is consistent with the model results.

#### 4. Summary and Discussion

Based on 45 year output data from historical, historical GHG, and historical Nat runs of 18 CMIP5 models, and the HadEX2 and CRU TS v.3.22 data sets, this study presents an evaluation of the climatology of the DTR and attempts to sort out the relative contributions of different forcings on the trend in the DTR over Asia. In a climatological mean sense, the MME of models generally reproduced the geographical distribution of the annual DTR over Asia and captured well the intensity of the DTR over eastern China (~10.5°C) and India (~12°C). However, compared with observations, the annual DTR of the MME was substantially underestimated over western China and north of 40°N in Asia. The intermodel spread was particularly large in arid and semiarid regions in Asia. Seasonal biases in the DTR from models were similar to the bias in the annual mean DTR. This suggests that

run may be caused by the compensating effects of aerosols' cooling and GHG warming. Underestimation of the urbanization effect over China might be a reason for the relatively weak warm trend in  $T_{\min}$  compared with that from observations. Anthropogenic aerosol forcing caused a negative trend in  $T_{\max}$  over south Asia but a large positive trend over north Asia.

This asymmetry may be partly due to the different effects of aerosols on  $T_{\max}$  and  $T_{\min}$ . Based on observations from two big cities and nearby mountains in China, aerosol direct effects on the  $T_{\max}$  and DTR trends were singled out. Long-term changes due to natural variability, greenhouse gases, should be similar between the city/mountain pairs of weather stations except for the level of local pollution at both locations. The two cities have experienced significant reductions in visibility due to scattering and/or absorption by aerosol particles whose effects are most notable during the daily peak in solar radiation. This serves to lower  $T_{\max}$ . As a result, the difference in  $T_{\max}$  between the cities and nearby mountains had significantly reduced. This is consistent with impact of increasing loading aerosols in China and can help explain the systematic difference in the trends in the DTR between the mountain and city stations.

The observed declining trend in the DTR at the decadal time scale may be driven not only by external forcing but also by internal variability. Because the analysis here is based on an MME, internal variability is weakened to a certain extent [Song *et al.*, 2014]. In our analysis, we have suggested that external forcing, especially anthropogenic forcing, plays a dominant role in the declining trend in the DTR over Asia. However, the decreasing trend in the DTR over the high latitudes of the Asian continent in models is weaker than what is seen in observations. This discrepancy may be related to internal variability. Thus, the contribution of internal variability on DTR trends deserves further study.

#### Acknowledgments

We thank the anonymous reviewers for their careful review and insightful comments. We acknowledge the climate modeling groups (listed in Table 1) for producing and making available their model output (<https://pcmdi.llnl.gov/search/cmip5/>). We also acknowledge the National Meteorological Information Centre for generating and making available their homogenized daily climate data from observation stations in China that can be obtained by contacting Mr. A. Xiong ([xay@cma.gov.cn](mailto:xay@cma.gov.cn)). This study was supported by the Ministry of Science and Technology (2013CB955804), NSF (91544217), NSF (AGS1534670), and the Humboldt Research Award to Z.L.

#### References

- Braganza, K., D. J. Karoly, and J. M. Arblaster (2004), Diurnal temperature range as an index of global climate change during the twentieth century, *Geophys. Res. Lett.*, *31*, L13217, doi:10.1029/2004GL019998.
- Collatz, G. J., L. Bounoua, S. O. Los, D. A. Randall, I. Y. Fung, and P. J. Sellers (2000), A mechanism for the influence of vegetation on the response of the diurnal temperature range to changing climate, *Geophys. Res. Lett.*, *27*(20), 3381–3384, doi:10.1029/1999GL010947.
- Dai, A., A. D. D. Genio, and I. Y. Fung (1997), Clouds, precipitation and temperature range, *Nature*, *386*(6626), 665–666.
- Dai, A., K. E. Trenberth, and T. R. Karl (1999), Effects of clouds, soil moisture, precipitation, and water vapor on diurnal temperature range, *J. Clim.*, *12*(8), 2451–2473.
- Donat, M. G., et al. (2013), Updated analyses of temperature and precipitation extreme indices since the beginning of the twentieth century: The HadEX2 dataset, *J. Geophys. Res. Atmos.*, *118*, 2098–2118, doi:10.1002/jgrd.50150.
- Gong, H., L. Wang, W. Chen, R. Wu, K. Wei, and X. Cui (2014), The climatology and interannual variability of the East Asian winter monsoon in CMIP5 models, *J. Clim.*, *27*(4), 1659–1678.
- Harris, I., P. D. Jones, T. J. Osborn, and D. H. Lister (2014), Updated high-resolution grids of monthly climatic observations—the CRU TS3.10 dataset, *Int. J. Climatol.*, *34*(3), 623–642.
- Intergovernmental Panel on Climate Change (IPCC) (2013), *Climate Change 2013: The Physical Science Basis. Contribution of Working Group I to the Fifth Assessment Report of the Intergovernmental Panel on Climate Change*, edited by T. F. Stocker, et al., 1535 pp., Cambridge Univ. Press, Cambridge, U. K., and New York, doi:10.1017/CBO9781107415324.
- Karl, T. R., R. W. Knight, K. P. Gallo, T. C. Peterson, P. D. Jones, G. Kukla, N. Plummer, V. Razuvayev, J. Lindsey, and R. J. Charlson (1993), A new perspective on recent global warming: Asymmetric trends of daily maximum and minimum temperature, *Bull. Am. Meteorol. Soc.*, *74*(6), 1007–1023.
- Karoly, D. J., K. Braganza, P. A. Stott, J. M. Arblaster, G. A. Meehl, A. J. Broccoli, and K. W. Dixon (2003), Detection of a human influence on North American climate, *Science*, *302*(5648), 1200–1203.
- Leibensperger, E. M., L. J. Mickley, D. J. Jacob, W. T. Chen, J. H. Seinfeld, A. Nenes, P. J. Adams, D. G. Streets, N. Kumar, and D. Rind (2012), Climatic effects of 1950–2050 changes in US anthropogenic aerosols. Part 2: Climate response, *Atmos. Chem. Phys.*, *12*(7), 3349–3362.
- Lewis, S. C., and D. J. Karoly (2013), Evaluation of historical diurnal temperature range trends in CMIP5 models, *J. Clim.*, *26*(22), 9077–9089.
- Li, J., et al. (2015), Aircraft measurements of the vertical distribution and activation property of aerosol particles over the Loess Plateau in China, *Atmos. Res.*, *155*, 73–86.
- Li, Z., F. Niu, J. Fan, Y. Liu, D. Rosenfeld, and Y. Ding (2011a), Long-term impacts of aerosols on the vertical development of clouds and precipitation, *Nat. Geosci.*, *4*(12), 888–894.
- Li, Z., et al. (2011b), East Asian Studies of Tropospheric Aerosols and their Impact on Regional Climate (EAST-AIRC): An overview, *J. Geophys. Res.*, *116*, D00K34, doi:10.1029/2010JD015257.
- Lindvall, J., and G. Svensson (2015), The diurnal temperature range in the CMIP5 models, *Clim. Dynam.*, *44*(1–2), 405–421.
- Meehl, G. A., W. M. Washington, C. M. Ammann, J. M. Arblaster, T. M. L. Wigley, and C. Tebaldi (2004), Combinations of natural and anthropogenic forcings in twentieth-century climate, *J. Clim.*, *17*(19), 3721–3727.
- Mitchell, T. D., and P. D. Jones (2005), An improved method of constructing a database of monthly climate observations and associated high-resolution grids, *Int. J. Climatol.*, *25*(6), 693–712.
- Ren, G., and Y. Zhou (2014), Urbanization effect on trends of extreme temperature indices of national stations over mainland China, 1961–2008, *J. Clim.*, *27*(6), 2340–2360.
- Ren, G., Y. Zhou, Z. Chu, J. Zhou, A. Zhang, J. Guo, and X. Liu (2008), Urbanization effects on observed surface air temperature trends in north China, *J. Clim.*, *21*(6), 1333–1348.
- Song, F., T. Zhou, and Y. Qian (2014), Responses of East Asian summer monsoon to natural and anthropogenic forcings in the 17 latest CMIP5 models, *Geophys. Res. Lett.*, *41*, 596–603, doi:10.1002/2013GL058705.

- Stenchikov, G. L., and A. Robock (1995), Diurnal asymmetry of climatic response to increased CO<sub>2</sub> and aerosols: Forcings and feedbacks, *J. Geophys. Res.*, *100*(D12), 26,211–26,227, doi:10.1029/95JD02166.
- Stone, D., and A. J. Weaver (2003), Factors contributing to diurnal temperature range trends in twentieth and twenty-first century simulations of the CCCma coupled model, *Clim. Dyn.*, *20*(5), 435–445.
- Stone, D. A., and A. J. Weaver (2002), Daily maximum and minimum temperature trends in a climate model, *Geophys. Res. Lett.*, *29*(9), 1356, doi:10.1029/2001GL014556.
- Sun, D., R. T. Pinker, and M. Kafatos (2006), Diurnal temperature range over the United States: A satellite view, *Geophys. Res. Lett.*, *33*, L05705, doi:10.1029/2005GL024780.
- Taylor, K. E. (2001), Summarizing multiple aspects of model performance in a single diagram, *J. Geophys. Res.*, *106*(D7), 7183–7192, doi:10.1029/2000JD900719.
- Taylor, K. E., R. J. Stouffer, and G. A. Meehl (2012), An overview of CMIP5 and the experiment design, *Bull. Am. Meteorol. Soc.*, *93*(4), 485–498.
- Vose, R. S., D. R. Easterling, and B. Gleason (2005), Maximum and minimum temperature trends for the globe: An update through 2004, *Geophys. Res. Lett.*, *32*, L23822, doi:10.1029/2005GL024379.
- Wang, F., C. Zhang, Y. Peng, and H. Zhou (2014), Diurnal temperature range variation and its causes in a semiarid region from 1957 to 2006, *Int. J. Climatol.*, *34*(2), 343–354.
- Wang, X. L. (2008a), Accounting for autocorrelation in detecting mean shifts in climate data series using the penalized maximal *t* or *F* test, *J. Appl. Meteorol. Climatol.*, *47*(9), 2423–2444.
- Wang, X. L. (2008b), Penalized maximal *F* test for detecting undocumented mean shift without trend change, *J. Atmos. Oceanic Technol.*, *25*(3), 368–384.
- Wang, X. L., Q. H. Wen, and Y. Wu (2007), Penalized maximal *t* test for detecting undocumented mean change in climate data series, *J. Appl. Meteorol. Climatol.*, *46*(6), 916–931.
- Yang, X., Z. Yao, and Z. Li (2013), Heavy air pollution suppresses summer thunderstorms in central China, *J. Atmos. Sol. Terr. Phys.*, 95–96, 28–40, doi:10.1016/j.jastp.2012.12.023.
- Zhou, L., R. E. Dickinson, Y. Tian, J. Fang, Q. Li, R. K. Kaufmann, C. J. Tucker, and R. B. Myneni (2004), Evidence for a significant urbanization effect on climate in China, *Proc. Natl. Acad. Sci. U.S.A.*, *101*(26), 9540–9544.
- Zhou, L., R. E. Dickinson, Y. Tian, R. S. Vose, and Y. Dai (2007), Impact of vegetation removal and soil aridation on diurnal temperature range in a semiarid region: Application to the Sahel, *Proc. Natl. Acad. Sci. U.S.A.*, *104*(46), 17,937–17,942.
- Zhou, L., R. Dickinson, P. Dirmeyer, H. Chen, Y. Dai, and Y. Tian (2008), Asymmetric response of maximum and minimum temperatures to soil emissivity change over the Northern African Sahel in a GCM, *Geophys. Res. Lett.*, *35*, L05402, doi:10.1029/2007GL032953.
- Zhou, L., R. E. Dickinson, P. Dirmeyer, A. Dai, and S.-K. Min (2009a), Spatiotemporal patterns of changes in maximum and minimum temperatures in multi-model simulations, *Geophys. Res. Lett.*, *36*, L02702, doi:10.1029/2008GL036141.
- Zhou, L., A. Dai, Y. Dai, R. Vose, C.-Z. Zou, Y. Tian, and H. Chen (2009b), Spatial dependence of diurnal temperature range trends on precipitation from 1950 to 2004, *Clim. Dyn.*, *32*(2–3), 441–441.
- Zhou, L., R. Dickinson, A. Dai, and P. Dirmeyer (2010), Detection and attribution of anthropogenic forcing to diurnal temperature range changes from 1950 to 1999: Comparing multi-model simulations with observations, *Clim. Dyn.*, *35*(7–8), 1289–1307.